Biochimica et Biophysica Acta 1797 (2010) 11–19

Contents lists available at ScienceDirect

Biochimica et Biophysica Acta

journal homepage: www.elsevier.com/locate/bbabio

D1 protein variants in Photosystem II from *Thermosynechococcus elongatus* studied by low temperature optical spectroscopy

Joseph L. Hughes [a,b,c,*], Nicholas Cox [c,1], A. William Rutherford [a,b], Elmars Krausz [c], Thanh-Lan Lai [b], Alain Boussac [b], Miwa Sugiura [d]

[a] Laboratoire d'Optique et Biosciences, INSERM U696 – CNRS UMR7645 Ecole Polytechnique, 91128 Palaiseau, France
[b] iBiTec-S, CNRS URA 2096, CEA Saclay 91191 Gif-sur-Yvette, France
[c] Research School of Chemistry, The Australian National University, Canberra, ACT 0200, Australia
[d] Cell-Free Science and Technology Research Center, Ehime University, Bunkyo-cho, Matsuyama, Ehime 790-8577, Japan

ARTICLE INFO

Article history:
Received 3 June 2009
Received in revised form 17 July 2009
Accepted 20 July 2009
Available online 27 July 2009

Keywords:
PheoD1
Primary donor
Side-pathway
Charge transfer transition

ABSTRACT

In Photosystem II (PSII) from *Thermosynechococcus elongatus*, high-light intensity growth conditions induce the preferential expression of the $psbA_3$ gene over the $psbA_1$ gene. These genes encode for the D1 protein variants labeled D1:3 and D1:1, respectively. We have compared steady state absorption and photo-induced difference spectra at <10 K of PSII containing either D1:1 or D1:3. The following differences were observed. (i) The pheophytin Q_x band was red-shifted in D1:3 (547.3 nm) compared to D1:1 (544.3 nm). (ii) The electrochromism on the $Pheo_{D1}$ Q_x band induced by Q_A^- (the C550 shift) was more asymmetric in D1:3. (iii) The two variants differed in their responses to excitation with far red (704 nm) light. When green light was used there was little difference between the two variants. With far red light the stable ($t_{1/2}$>50 ms) Q_A^- yield was ~95% in D1:3, and ~60% in D1:1, relative to green light excitation. (iv) For the D1:1 variant, the quantum efficiency of photo-induced oxidation of side-pathway donors was lower. These effects can be correlated with amino acid changes between the two D1 variants. The effects on the pheophytin Q_x band can be attributed to the hydrogen bond from Glu130 in D1:3 to the 13^1-keto of $Pheo_{D1}$, which is absent for Gln130 in D1:1. The reduced yield with red light in the D1:1 variant could be associated with either the Glu130Gln change, and/or the four changes near the binding site of P_{D1}, in particular Ser153Ala. Photo-induced Q_A^- formation with far red light is assigned to the direct optical excitation of a weakly absorbing charge transfer state of the reaction centre. We suggest that this state is blue-shifted in the D1:1 variant. A reduced efficiency for the oxidation of side-pathway donors in the D1:1 variant could be explained by a variation in the location and/or redox potential of P^+.

1. Introduction

The membrane-bound protein complex Photosystem II (PSII) is a light-driven Water:Plastoquinone Oxidoreductase [1] and is the first stage of the bioenergetic electron transfer chain in oxygenic photosynthesis. Visible light excitation of chlorophyll (Chl) pigments drives electron transfer processes between the redox components of the PSII reaction center, which are mostly bound to the D1 protein. PSII performs the four-electron oxidation of substrate water at the Mn_4Ca oxygen-evolving complex on the luminal side of the membrane and the two-electron reduction of the exchangeable quinone acceptor (Q_B) at the stromal side.

Light excitation of the primary electron donor P, a Chl assembly, initiates electron transfer along the reaction center D1 protein branch, where a pheophytin ($Pheo_{D1}$) is the first electron acceptor. This results in the charge-separated state $P^+Pheo_{D1}^-$, with subsequent electron transfer from $Pheo_{D1}^-$ to the first quinone acceptor, Q_A, followed by Q_A^- to Q_B transfer. Two sequential primary electron transfer events result in the two-electron reduction of Q_B, which is released to the stroma as a quinol (Q_BH_2) after proton uptake, and then replaced with a new quinone from the pool. The oxidized primary donor state, P^+, oxidizes the redox active tyrosine, Tyr_Z, and the tyrosyl radical formed then oxidizes the Mn_4Ca cluster. After four sequential photochemical events resulting in the accumulation of four positive charge equivalents at the Mn_4Ca site, two substrate water molecules are oxidized, with the release of molecular oxygen and four protons.

Unlike plants and algae, which have only one gene copy encoding for the D1 protein, cyanobacteria have small gene families that code for D1 protein variants. In *Thermosynechococcus elongatus* (*T. elongatus*), three different genes ($psbA_1$, $psbA_2$, $psbA_3$) encode for three different D1 protein isoforms [2]. By analogy to other cyanobacteria, environmental

* Corresponding author. Laboratoire d'Optique et Biosciences, INSERM U696 – CNRS UMR7645 Ecole Polytechnique, 91128 Palaiseau, France. Tel.: +33 1 6933 5049; fax: +33 1 6933 5084.
E-mail address: joseph.hughes@polytechnique.edu (J.L. Hughes).
[1] Current address: MPI für Bioanorganische Chemie, Stiftstrasse 34-36/D-45470 Mülheim an der Ruhr, Germany.

0005-2728/$ – see front matter © 2009 Elsevier B.V. All rights reserved.
doi:10.1016/j.bbabio.2009.07.007

stress conditions can be expected to induce the differential expression of these D1 isoforms [3–9]. Recently, high-light conditions have been shown to preferentially induce the expression of the *psbA*$_3$ gene over *psbA*$_1$ in *T. elongatus* (*psbA*$_2$ expression is negligible under the conditions studied) [10–13]. This acclimation has been associated with a photoprotective role [6,12,14,15]. The yield of radical pair formation and charge recombination processes are both key components in PSII photoprotection mechanisms. In light of this, the current paper focuses on differences between the D1:1 and D1:3 variants in (i) the spectral properties of the Pheo$_{D1}$, (ii) phenomena associated with the primary donor and (iii) the electron transfer side-pathway at low temperatures.

1.1. Pheo$_{D1}$

In the low-light D1:1 and high-light D1:3 variants, the residues at D1–130 are glutamine and glutamate, respectively. These residues are within hydrogen-bonding distance to the 13^1-keto of Pheo$_{D1}$, and the glutamate will be capable of providing such an interaction [13]. In cyanobacteria, the high-light D1 variants typically contain glutamate at position D1–130 [3,6,16]. The residue at D1–130 in plants and algae is exclusively glutamate.

A hydrogen bond to the 13^1-keto of Pheo$_{D1}$ has been associated with modulation of the ΔG between $P^+Pheo_{D1}^-$ and P* [12,17,18]. From fluorescence yield and thermoluminescence studies on *T. elongatus* Kós et al. [12] recently proposed that accelerated $S_2Q_A^-$ and $S_2Q_B^-$ charge recombination was associated with increased expression of the D1:3 isoform. These results were interpreted as an increased free energy gap between P* and $P^+Pheo_{D1}^-$. The yield of radical pair formation and the role of charge recombination in photoprotection were related to high-light acclimation and differential *psbA* expression.

1.2. The primary donor and optically accessible charge transfer transitions

Hughes et al. [19] recently reported a low energy (700–730 nm), weak absorption band in higher-plant PSII that was attributed to an optically accessible charge transfer (CT) transition of the reaction center. The absorption intensity of this CT band was suggested to be due to mixing with the Q$_y$ transitions of the two pigments for which there is direct electronic overlap, the special pair P$_{D1}$–P$_{D2}$. Models describing the pigment electronic structure and/or primary light-induced energy and electron transfer dynamics in PSII now incorporate at least two radical pair states of the reaction center chromophores [20–26]. The recent model of Novoderezhkin et al. [23] explicitly incorporates optical CT states. Their model identified a CT transition which they associated with the 700–730 nm state observed by Hughes et al. [19] for higher-plant PSII.

1.3. The side-pathway

Upon lowering the temperature, photo-induced electron transfer from the catalytic oxygen-evolving tetranuclear Mn cluster to the oxidized primary donor, P^+, is inhibited [27]. Under these conditions a side-pathway can operate where alternative terminal electron donors are oxidized, including chlorophyll (ChlZ), β-carotene (Car), and when in the reduced form, the heme group of cytochrome *b*$_{559}$ (Cyt*b*$_{559}$) [28,29]. A Car on the D2 side of the reaction center is the branch point in this side-pathway model [29,30] and acts as the immediate electron donor to P^+. Car^+ can be re-reduced by either Cyt*b*$_{559}$ or ChlZ.

The Car, ChlZ and Cyt*b*$_{559}$ side-path donors are believed to have a physiologically relevant protective role either by providing electrons to $P680^+$ under conditions where the usual donors are oxidized [28] or by maintaining the Car on the D2 branch in the neutral form so that it is available to quench photo-generated triplet Chl species and $^1O_2$ [29]. There is a very wide distribution of quantum efficiencies for terminal oxidation of the side-pathways donors at 8 K, at minimum spanning values from 0.2 to 0.014 [31].

1.4. Optical spectroscopy of D1 variants

In this work we used steady state absorption spectroscopy and photo-induced difference spectroscopy at temperatures below 10 K to investigate the suggestion [13] that hydrogen bonding due to Glu130 may modify the protein interaction at the 13^1 keto of Pheo$_{D1}$. We examined the effect of illuminating the D1:1 and D1:3 variants at 8 K with far red (704 nm) light, which excites an optically accessible CT state of the reaction center, compared to green light which initiates charge separation in PSII via Q$_y$ excitations of the pigments. We also investigated whether there is an effect on the yield and quantum efficiency distribution of terminal side-pathway oxidation following green light illumination of these variants.

2. Materials and methods

2.1. Preparation of PSII core complexes (D1:1 and D1:3 samples) from T. elongatus

Construction of *T. elongatus* His$_6$-tag on C-terminus of CP43 strain (43-H) [32] and Δ*psbA*$_1$, Δ*psbA*$_2$, His$_6$-tag on the C-terminus of CP43 strain (WT*) [33] have been described previously. In the present work, to indicate the D1-variant, the 43-H and WT* preparations are referred to as D1:1 and D1:3, respectively. Purification of the PSII core complexes was also as described previously [33].

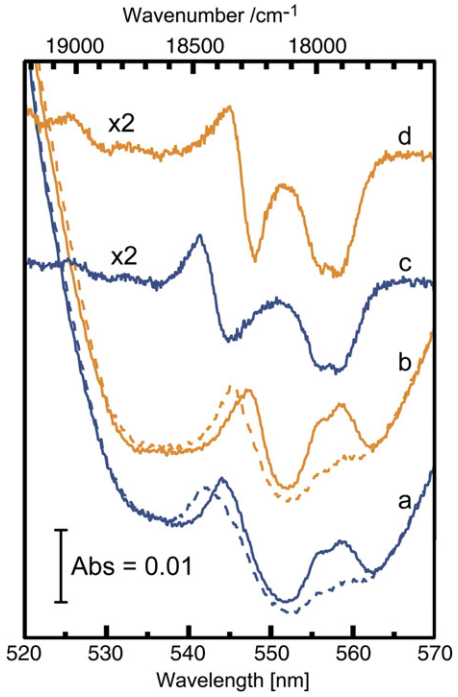

Fig. 1. Absorption spectra (traces (a) and (b)) of *T. elongatus* PSII core complex D1:1 (blue in online version) and D1:3 (yellow in online version) samples at 1.4 K in the Pheo Q$_x$ region. The traces are offset along the *y*-axis for clarity. The absorption spectra were measured before (solid lines) and after (dotted lines) illumination at 1.4 K with 100 mJ/cm^2 of 514 nm light (20 s, 5 mW/cm^2). The corresponding after-minus-before illumination Δ*A* difference spectra are also presented as traces (c) and (d), and identify the derivative-shaped 'C550' electrochromic shift of the Pheo$_{D1}$ in each sample. The α Q-band of the reduced heme of Cyt*b*$_{559}$ is also observed centered at 557 nm, and appears as a bleach in the Δ*A* difference spectra due to its oxidation.

2.2. Preparation of samples for optical measurements

For optical measurements, samples were diluted in a medium containing 1 M betaine, 15 mM $CaCl_2$, 15 mM $MgCl_2$, 40 mM Mes (pH 6.5 adjusted with NaOH), 25% glycerol and 25% ethylene glycol (% by volume) as a glassing medium. The sample was then syringed into a ~200 μm path-length quartz-windowed cell assembly [34]. The cell assembly was attached to the sample rod, which was inserted into an isolated-environment lock chamber attached to the cryostat and then dark-adapted for ~40–50 min at room temperature to allow relaxation to the $S1Q_A$ configuration. The lock chamber was then opened and the sample rod lowered into the cryogen, where cooling to below 130 K took less than 3 min.

2.3. Optical measurements

The absorption-difference spectra we report in this work were those measured after a controlled external illumination, minus the 'dark' spectrum measured before any external illumination. The scanning monochromator [35] and CCD-based spectrometers [36] were used as described previously [31]. The data presented in Fig. 1 used the scanning monochromator spectrometer, and the data are not limited by the instrument spectral resolution. The data in Figs. 2 and 3 used the CCD-based spectrometer, which allow detailed kinetic measurements. For this work, we used a 10 ms gate for the CCD spectrometer absorption measurements, the spectra were collected at a rate of 0.2 Hz, and the time period from cessation of the external illumination to the absorption measurement was of the order 50 ms. The measurement light of the CCD-based spectrometer does not induce any detectable Q_A^- formation or side-path oxidation for the spectra reported here, as quantified previously [31].

The degrees of photo-induced Q_A^- formation and side-path oxidation were quantified as previously described [31]. Briefly, the $Pheo_{D1}$ Q_x electrochromic shift (C-550) was used to indicate Q_A^- formation, and the extinction coefficients for Car^+ absorption at ~1000 nm and the reduced form of the heme in $Cytb_{559}$ at ~557 nm ($Cytb_{559}^{reduced} - Cytb_{559}^{oxidized}$ difference extinction coefficient) were taken as 130×10^3 and 41×10^3 M^{-1} cm^{-1}, respectively (see [31] and

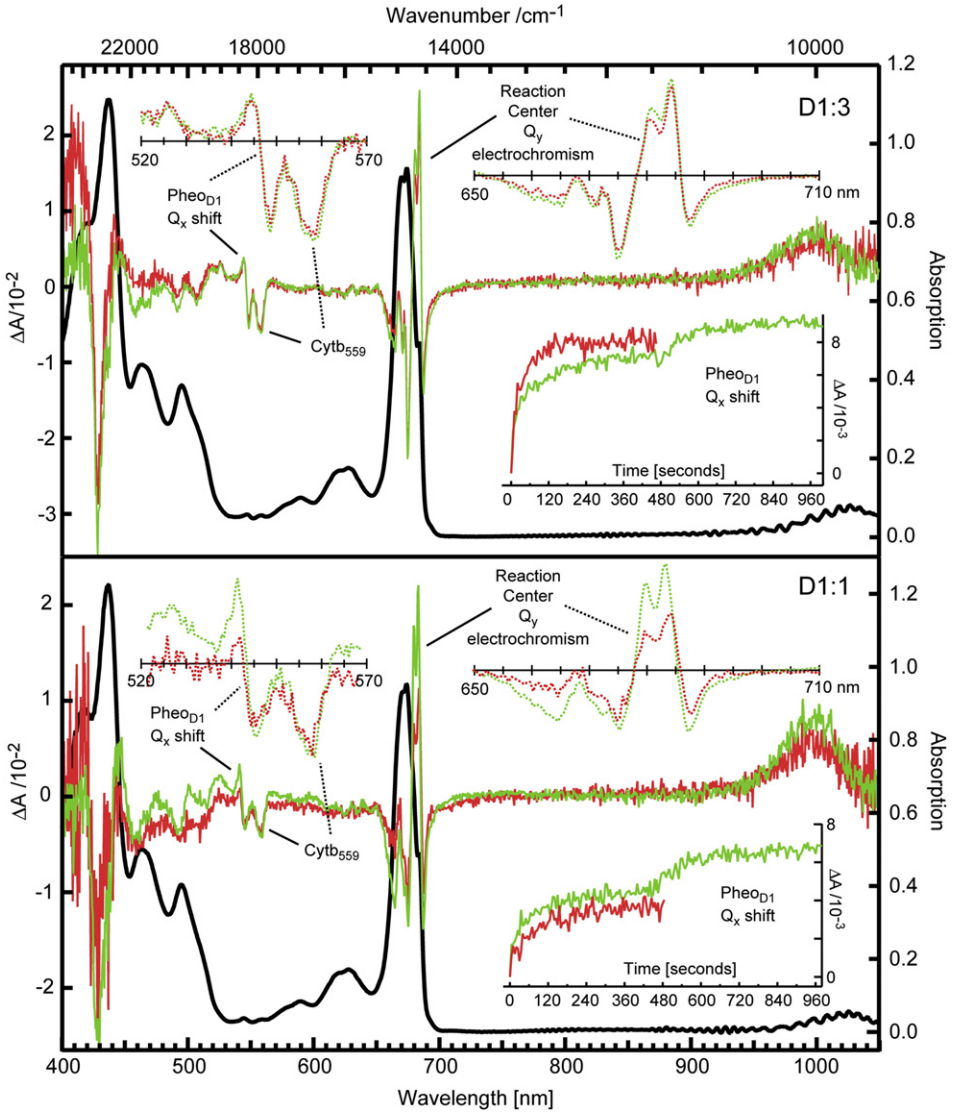

Fig. 2. Absorption spectra at 8 K of *T. elongatus* PSII core complex D1:1 (lower panel) and D1:3 (upper panel) variants before any illumination (black traces). The fringing pattern at λ > 800 nm, and apparent absorption near 1030 nm are artifacts that do not affect the Δ*A* spectra (see text). The light grey and dark grey traces (green and red in online version) show the after-minus-before illumination Δ*A* spectra obtained following 514 nm (0.01 mW/cm^2 for 460 s, plus 1 mW/cm^2 for 510 s) and 704 nm (10 mW/cm^2 for 480 s) excitation, respectively. These illuminations were performed on separate dark-adapted samples, and have been scaled to the same sample concentration. The regions in the Δ*A* spectra identifying Q_y electrochromism (top right inserts) and the $Pheo_{D1}$ Q_x electrochromic shift and oxidation of $Cytb_{559}$ (top left inserts) have been expanded for clarity. The bottom right inserts show the peak-to-peak amplitude of the $Pheo_{D1}$ Q_x Δ*A* as a function of illumination time (see text for details).

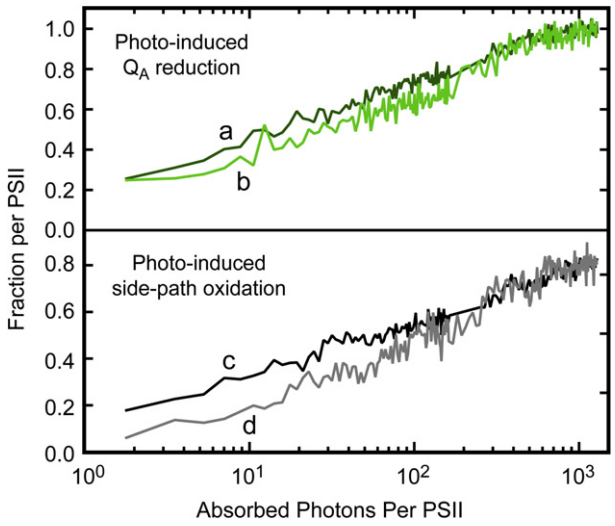

Fig. 3. Photo-induced Q_A reduction (top panel) and side-path donor oxidation (bottom panel) for the D1:3 sample, dark traces (a) and (c) and the D1:1 sample, light traces (b) and (d). Illumination was with 514.5 nm light. The side-path oxidation for the D1:1 variant (d) has been scaled by ×1.23 for a direct qualitative comparison of the quantum efficiency distribution with D1:3 (c).

references therein for more detailed discussion of the estimates for these extinction coefficients). The net area of the Q_y absorption was also monitored, and a net loss of area was used as a measure of Chl oxidation.

2.4. Sample illumination

Two different laser systems were used for controlled sample illumination. For green light illumination, the 514.5 nm line of a Spectra Physics model 165 Ar^+ laser was defocused to ensure uniform illumination of the sample. For 704 nm illuminations, a Spectra Physics model 375 dye laser operating with DCM dye and pumped by a Spectra Physics model 175 Ar^+ laser was used. A 3-plate birefringent filter was used for wavelength selection, resulting in a linewidth of ~1–2 cm^{-1}. The output of the dye laser was propagated ~8 m from a Littrow reflector to separate the laser light from the fluorescence background of the DCM dye. Neutral density filters were used to reduce the power as required.

3. Results

3.1. D1-variant effect on Pheo Q_x absorption and 'C-550' shift

Fig. 1 shows the 520–570 nm absorption region of PSII core complexes from *T. elongatus*, containing either D1:1 or D1:3 protein variants. The spectra are scaled to the same sample concentration, as determined by the area of the Q_y absorption bands. The absorption spectra before and after illumination with 514.5 nm light are shown as the solid and dotted lines in traces (a) and (b). The α Q-band absorption of the reduced heme of Cytb_{559} is centered at ~557 nm (Fig. 1) in both D1:1 and D1:3 samples (traces (a) and (b), Fig. 1). The near-degenerate Q_x and Q_y transitions of reduced Cytb_{559} are resolved in the double-peaked ~557 nm absorption band. In the dark spectra (solid lines, (a) and (b)), the peak of the Pheo Q_x absorption is at 544.3 nm and 547.3 nm for the D1:1 and D1:3 samples, respectively. The red shift of the Pheo Q_x absorption peak by 3.0 nm for the D1:3 sample, relative to the D1:1 sample, is assigned to the hydrogen bond to the ^{1}13-keto of the $Pheo_{D1}$ from the carboxylate group of Glu130 in D1:3. This is consistent with mutagenesis studies which have identified that the Q_x bands for the bacteriopheophytin in the active L-branch of the Bacterial Reaction Center (BRC) [37] and for $Pheo_{D1}$ in PSII from *Synechocystis* PCC 6803 [38,39] red shift due to a hydrogen bond to the 13^1-keto ring substituent.

The after-minus-before illumination absorption-difference spectra are also presented in Fig. 1 as traces (c) and (d), showing the electrochromic blue shift of the $Pheo_{D1}$ Q_x absorption dominated by the presence of Q_A^-, known as the C-550 shift. The profiles of the $Pheo_{D1}$ Q_x Δ*A* spectra for the D1:1 and D1:3 samples are distinctly different. The Δ*A* spectrum of the D1:1 sample has a nearly symmetric derivative shape, whereas that for the D1:3 sample exhibits significant asymmetry. This asymmetry is also observed for the $Pheo_{D1}$ Q_x shift measured, at least in some cases, in higher plants [19,40,41] and can be correlated with the presence of the hydrogen bond from D1-Glu130 to the ^{1}13-keto of $Pheo_{D1}$.

There are weak, positive features in the Δ*A* spectra at 532.7 nm and 525.6 nm. These features appear in both D1:1 and D1:3 samples, and are not associated with the shift of either of the pheo absorptions. These weak features exhibit different amplitudes in the D1:1 and D1:3 samples, and scale with the different amplitudes of the Cytb_{559} absorption bleaches centered at ~557.4 nm. Thus, these weak, positive features might be associated with absorptions of an oxidized form of the heme in Cytb_{559} [42]. They do not account for the asymmetry in the $Pheo_{D1}$ Q_x electrochromism for the D1:3 sample.

The significant asymmetry of the $Pheo_{D1}$ Q_x shift suggests either (i) an intrinsically asymmetric absorption profile, (ii) a change in absorption intensity, or (iii) a change in width. An intrinsic asymmetric profile has recently been attributed to the $Pheo_{D1}$ Q_x absorption in higher plants, and suggested to be due to phonon sideband intensity [41]. A variation in this sideband intensity may be associated with vibronic coupling of the Q_x state with other electronic states. Vibrational sideband intensities of the Q_y transition of protein-bound Chl *a* have been shown to be variable [43]. A change in width might also be associated with the interplay between Stark effects associated with changes in dipole moment (Δμ) and polarizability (Δα) [44].

From the higher-plant electrochromic data [41] a broad higher-energy component of the asymmetric $Pheo_{D1}$ Q_x absorption was observable in the Δ*A* spectrum. A corresponding broad higher energy component is not clearly identifiable in the $Pheo_{D1}$ Q_x Δ*A* spectra presented here, for either the D1:1 or the D1:3 variants. In the present work we were unable to model the pheo absorption profiles, as accurate determination of the baseline was not possible due to the absorption changes in the 520–535 nm region due to Cytb_{559} oxidation (see above). Further data on the *T. elongatus* D1:1 and D1:3 variants in which Cytb_{559} is fully pre-oxidized will facilitate such an analysis, and may help to discriminate between the possibilities (i)–(iii) outlined in the previous paragraph.

The D1:3 sample was obtained from *T. elongatus* grown from a strain where the $psbA_1$ and $psbA_2$ genes were deleted, while the D1:1 sample used growth conditions that are considered to result in predominantly $psbA_1$ expression. The distinctly different positions and profiles of the $Pheo_{D1}$ Q_x shifts for D1:1 and D1:3 samples allows us to put quantitative limits on the proportion of the two types of reaction centre present: the D1:1 sample used here contained no more than 5% of centers bearing a D1:3 protein. This was determined by subtraction of the Δ*A* spectrum for the D1:3 sample from the Δ*A* spectrum for the D1:1 sample. For this subtraction, if the D1:3 Δ*A* spectrum was scaled to a sample concentration any more than ~5% of the D1:1 sample concentration, the result was a spectrum that was no longer smooth continuous, and an anomalous 'kink' appeared at 548 nm. This quantification is consistent with the recent analysis of the mRNA pool by Loll et al. [13] where the material used for crystallography grown under low-light conditions, and harvested late in the cell culture, contained <2% $psbA_3$. At earlier stages of cell culture, grown under low-light conditions, the mRNA level of $psbA_3$ increased to a maximum of 10%. Thus, although an increased mRNA level of $psbA_3$ under such conditions does not necessarily mean there

will be a corresponding increase in the expression of D1:3, the quantification using our optical results indicates that it is not detectable under our culture conditions.

3.2. Photo-induced Q_A reduction and side-path oxidation: 704 nm vs 514 nm excitation at 8 K

Fig. 2 shows the absorption spectra of D1:1 and D1:3 samples at 8 K before any illumination (black traces) over the full 400–1050 nm range. The spectra are dominated by Chl and Car absorption. The fringing pattern evident at wavelengths longer than ~800 nm is due to etaloning within the CCD detector chip. This fringing pattern is constant and thus does not affect the ΔA spectra. The feature beyond ~1000 nm is due to second order ~500 nm light. Since the absorption changes near 500 nm are small ($\Delta A/A<10\%$) and much narrower than the Car^+ absorption near 1000 nm, this process clearly has negligible affect on the ΔA spectra at wavelengths shorter than 1000 nm.

The after-minus-before illumination difference-spectra are shown in Fig. 2 as the green and red traces, corresponding to 514 and 704 nm illumination at 8 K, respectively. For illumination at 514 nm, each sample received the same irradiation dose. The 704 nm illumination for each sample was also with the same irradiance, although different to that used for 514 nm illumination (see figure legend). Accurate quantification of the absorbed fluence at 704 nm could not be made in this work, as addressed in the Results section "Yields of photo-induced Q_A reduction: the D1:3 variant." The sample concentrations were within ±10% of each other, and all the ΔA spectra as well as the kinetic traces (see below) have been normalized to the same concentration, as determined by the dark spectra (black traces) for the respective samples.

Illumination of either sample resulted in the appearance of a Car^+ absorption near 1000 nm and depletion of Car absorption in the 450–520 nm range. There was also absorption depletion due to oxidation of the initially reduced Cytb_{559}, as for the data in Fig. 1. The loss of Chl *a* absorption, determined by the net area of the ΔA spectra in the Q_y (0,0) region was inferred to indicate Chl oxidation. The ΔA spectra showing the electrochromism of the Chl/Pheo $Q_y(0,0)$ and $Pheo_{D1}$ Q_x absorptions that are due to Q_A^- and oxidized terminal side-path donors have been expanded for clarity of presentation, and are shown as the dotted traces inserted top right and left in Fig. 2. There are some small variations between the ΔA spectra observed at wavelengths shorter than 520 nm. These are minor artifacts associated with the baseline stability and the sensitivity of this particular wavelength region to the precise alignment of any optical components in the measurement light path of the CCD-based spectrometer.

The bottom right inserts in Figs. 2 and 3 show the growth of the peak-to-peak ΔA of the $Pheo_{D1}$ Q_x electrochromic shift, which monitors trapped ($t_{1/2}$>50 ms) Q_A^- as a function of illumination time for excitations at 704 nm and 514 nm. The ΔA spectra that are presented in Fig. 2 correspond to the endpoints of the kinetics shown in the inserts. These correspond to saturating illuminations, where the maximum possible (within 5%) photo-induced Q_A reduction with the respective illumination wavelengths was obtained [19,31]. For the 514 nm illuminations, two irradiances were used. The first illumination period (before ~480 s) used an irradiance of ~0.01 mW/cm^2, while the second period (after ~480 s) used ~1 mW/cm^2.

3.3. Yields of photo-induced Q_A reduction: the D1:3 variant

The ΔA spectra for the D1:3 samples obtained after saturating 514.5 nm and 704 nm illuminations, where longer illumination has negligible effect, are practically identical. The 704 nm illumination resulted in >90% of photo-induced Q_A^- formation relative to the 514 nm illumination, as determined by the peak-to-peak ΔA magnitude of the $Pheo_{D1}$ Q_X shift. Saturation of the $Pheo_{D1}$ Q_x ΔA was obtained by the illumination at 704 nm, as shown in the insert of Fig. 2.

Since these illuminations and measurements were performed at 8 K, the available thermal energy is kT~5.6 cm^{-1}. Consequently thermal activation by 28 cm^{-1} (5 kT) will occur in <1% of centers. Thus, thermal activation of absorption more than 1.5 nm to shorter wavelength than the excitation wavelength of 704 nm can be neglected. The bandwidth of the dye laser used for 704 nm excitation was ~1–2 cm^{-1}, and control experiments (see Materials and methods) demonstrated that the measurement light of the CCD-based spectrometer did not contribute to the photo-induced Q_A reduction or side-path oxidation for the data presented here. For the sample concentrations used in this work, the long-wavelength Chl absorption of the CP47 proximal antenna has been shown to be negligible at wavelengths longer than 704 nm in PSII core complexes isolated from spinach [45]. The very close correspondence evident between the long-wavelength CP47 absorption in spinach and *T. elongatus* (comparison not shown), allows us to suggest the same lower wavelength limit for any pigment absorptions in *T. elongatus*.

These results for the D1:3 variant demonstrate the existence of a state that absorbs at 704 nm and whose excitation at 8 K results in photo-induced Q_A reduction and side-path oxidation in practically all centers. This indicates that this low energy absorption band is dominantly homogeneously broadened, and we assign this species to an optically accessible CT state of the reaction center, analogous to that of plant PSII [19,46,47]. We have not as yet been able to quantify the absorption profile of this band in D1:3 samples from *T. elongatus*. This is due to the lower sample concentrations available in this work compared to the concentrated plant PSII core complex samples [19,45,47–49].

Our assignment of a weak low energy absorption band (>700 nm) to a CT transition is predicated on the observation that it is dominantly homogeneously broadened and its excitation leads to Q_A^- formation. The absorption band of a CT transition can be expected to have a dominant homogeneous component due to the excitation of multiple quanta of vibrational/phonon modes that accommodate the significant nuclear displacements associated with the charge transfer. Consequently, narrowband excitation within such an absorption band will result in absorption in a majority of centers. By contrast, absorption bands of long-wavelength Chl pigment transitions are typically dominated by inhomogeneous broadening, as demonstrated by spectral hole-burning measurements [45,47,49,50].

Both the irradiance and illumination times used in this work were comparable to those used for the illuminations near 704 nm of higher-plant PSII performed by Hughes et al. [19]. However, the plant PSII samples were more concentrated by a factor of ~×2–3, which allowed the identification of the 700–730 nm absorption band. The irradiance used was not indicated in the original paper [19], but was typically ~10–20 mW/cm^2 for illuminations near 705 nm. In higher plant, ~75% Q_A^- formation was achieved with 704 nm illumination [19], compared to ~95% for the *T. elongatus* PSII D1:3 variant (this work). In the higher-plant system, 704 nm illumination was reported to exhibit quantum efficiencies significantly lower than observed for green light (non-selective) illumination [19]. Thus, even though we cannot quantify the efficiencies in this work for 704 nm illuminations of our *T. elongatus* samples, they appear to be comparable to that observed for higher plants. For the higher-plant data [19], a scanning monochromator system was used to read out the C-550 shift for quantification of Q_A reduction. The slower readout inherent with this technique (~5 min) compared to the ~50 ms resolution used here for the CCD-based spectrometer means that recombination processes with $t_{1/2}$ of the order 5 min or less [19,31] may have contributed to the lower yield reported in the higher-plant data.

3.4. Yields of photo-induced Q_A reduction: the D1:1 variant

The ΔA spectra for the D1:1 samples obtained after saturating 514.5 nm and 704 nm illuminations exhibit significant differences in the yield of photo-induced Q_A reduction and side-path oxidation. The ΔA spectral profiles are very similar, but the amplitude of the electrochromism ΔA features are smaller by ~40% for the saturating 704 nm illumination, compared to the saturating 514.5 nm illumination.

As for the D1:3 sample, we attribute a homogeneously broadened CT absorption in the D1:1 variant whose excitation gives rise to Q_A reduction. However the yield of photo-induced Q_A^- formation by excitation at 704 nm of the D1:1 variant is markedly different to that for D1:3. In plant PSII, illuminations at progressively longer wavelengths beyond 700 nm led to a reduction in quantum efficiency of photoreduction [19]. From the kinetic traces in Figs. 2 and 3 both the quantum efficiency and the yield of 704 nm photo-induced Q_A^- reduction in the D1:1 variant are significantly lower than in D1:3.

In the dark absorption spectrum of the D1:1 sample, there was a weak, broad feature in the 700–730 nm region that was not evident in the D1:3 samples. Following the 704 nm illumination of the D1:1 sample there was some reduction of this absorption, but virtually no change following 514 nm illumination. Absorption depletion of the long-wavelength CT band in the 700–730 nm range in plant PSII following optical excitation at low temperature has been correlated with Q_A^- formation [19,45,48]. However, further experimentation is required to clarify and quantify whether this weak absorption in the D1:1 sample can be associated with the PSII reaction center.

3.5. Yields and quantum efficiencies of side-path oxidation: D1:1 vs D1:3 variants

The percentage yields per PSII for photo-induced oxidation of the terminal side-path donors for the saturating (maximum Q_A^-) 514 nm and 704 nm illuminations are presented in Table 1. As found previously [31], there appears to be a side-path donor that does not exhibit a clear spectral signature in the 400–1000 nm range. After a saturating green (514 nm) illumination, the total number of centers where terminal oxidation of the observed side-path donors occurred was ~65% for the D1:1 and ~80% for the D1:3 variants. In the D1:1 sample there was initially a lower amount of reduced Cytb_{559}, but in this case neither ChlZ nor Car replaced the Cytb_{559} as the terminal donor, i.e. there is more unidentified donor in the D1:1 sample. The amount of Car and ChlZ oxidation in both samples for saturating green illuminations was approximately the same. For D1:3, the distribution of oxidized side-path donors per Q_A^- was the same for the saturating 704 and 514 nm illuminations. After a saturating 704 nm illumination of the D1:1 sample there was a diminished amount of ChlZ oxidation per Q_A^-. This reduction was matched by an increased amount of unidentified donor, compared to the green illumination.

We reported [31] photo-induced Q_A reduction and terminal side-path donor oxidation in PSII isolated from *T. elongatus* from cultures grown with both *psbA*$_1$ and *psbA*$_3$ genes intact. This data was quantified as a function of absorbed photons per center [31]. A simple model was used to analyze the data where distinct quantum efficiency distributions were used to describe photo-induced Q_A reduction and terminal side-path oxidation. The photo-induced Q_A reduction was describable by three distinct quantum efficiency fractions: (i) a very high efficiency fraction with quantum efficiency ~0.5–1, (ii) a middle efficiency fraction having a very large quantum efficiency range of ~0.014–0.2 and (iii) a low efficiency fraction with quantum efficiency ~0.002. The side-path donors ChlZ, Car and reduced Cytb_{559} accounted quantitatively for the middle efficiency component.

Table 1
Photo-induced yields per PSII.

Sample	D1:3		D1:1	
Excitation	704 nm	514 nm	704 nm	514 nm
Q_A^-	95%	100%	60%	100%
Cyt$b_{559}^{(ox)}$	38%	40%	17% (26%)	28%
Car^+	11%	13%	10% (16%)	14%
Chl^+	26%	28%	10% (16%)	24%

The figures in brackets are normalized per Q_A^- for the corresponding 514 nm illumination.

For 514 nm illuminations of the D1:1 and D1:3 samples, we quantified as a function of the absorbed photons per PSII the photo-induced Q_A^- reduction and side-path donor oxidation that are presented as kinetics in the inserts of Fig. 2. The quantification is shown in Fig. 3. Only the summed side-path donor contributions are presented, as the current data sets are not able to provide meaningful conclusions regarding any distinctions between the quantum efficiency distributions for terminal oxidation of the different side-path donors. The results in Fig. 3 are in general quantitative agreement with those reported earlier [31], but with some notable variations.

The data in Fig. 3 have been scaled to the same endpoint so as to directly compare the functional form of the quantum efficiency curves, as this is a direct qualitative comparison of the distribution of quantum efficiencies. The initial data points for Q_A reduction in the two D1 variants are almost identical, indicating the same fraction of very high efficiency centers. These centers were previously ascribed to Tyr_Z oxidation [31]. The D1:1 variant exhibits a reduction in the broadly distributed middle quantum efficiency component of photo-induced Q_A reduction. This is accounted for by a change in the quantum efficiency distribution for oxidation of the side-path donors, where there are less centers in the higher efficiency fraction of the broad distribution (Fig. 3).

We point out that our analysis does not consider any fraction of PSII cores that may exhibit reversible photochemistry, i.e. generating the PQ_A ground state from photo-induced $P^+Q_A^-$ (recombination $t_{1/2}$~2 ms). However, as quantified previously [19,31], the maximum amount of Q_A^- per PSII induced by low temperature illumination in our samples is considered to be $95 \pm 5\%$, indicating that the fraction of centers that might only perform such reversible photochemistry is negligible in the experiments reported here. Competition of side-path oxidation with $P^+Q_A^-$ recombination accounts in part for the low efficiencies of photo-induced side-path oxidation.

4. Discussion

4.1. Optically accessible CT transitions of the reaction center

There are a number possible charge-separated configurations of the reaction center pigments of PSII. This is reflected in descriptions of the electronic structure and electron transfer dynamics of the PSII reaction center. Current models introduce a number of radical pair states associated with the primary charge separation kinetics [20–26]. Significant optical intensity (i.e that approaching the absorption intensity of Chl Q_y) in a CT band requires a substantial degree of electronic overlap between the donor and acceptor. From PSII structural data [51,52], only the P_{D1} and P_{D2} special pair pigments are close enough to allow an appropriate level of electronic overlap.

We note that theoretical studies of the bacterial reaction center (BRC) have been unequivocal in excluding any significant CT intensity involving pigments apart from the special pair of bacteriochlorophylls [53]. The center-to-center separation of the special pair pigments in PSII (7.6 Å) [51] is almost the same as that in the BRC (7.5 Å). The intensity of the CT band in higher-plant PSII has been estimated as equivalent to $\sim 0.15 \pm 0.05$ of the Chl *a* Q_y transition [19] and this is close to the value of the absorption intensity calculated for the CT band in the BRC.

Over the past decade, a consensus has emerged that primary charge separation in PSII is initiated at Chl_{D1}, rather than P_{D1}/P_{D2} [22,54–61]. This is in agreement with the original proposal [62], based

on the location of the PSII reaction center triplet state on Chl_{D1}. One inference from the work presented here is that the charge-separated state relating to the putative low energy CT absorption at $\lambda > 700$ nm might be expected to contain significant $Chl^{+}_{D1}Pheo^{-}_{D1}$ character. However, this possibility is contraindicated by the lack of significant electronic overlap between these pigments (see above). An optically accessible P_{D1}–P_{D2} CT band may not only have P_{D1}/P_{D2} pigment character via mixing with their Q_y excitations, but also gain some component of Chl_{D1} character by exciton coupling processes between the reaction centre pigments [19,23]. Excitation of this small component of Ch_{D1} Q_y character in the CT transition may then proceed to $Chl^{+}_{D1}Pheo^{-}_{D1}$ charge separation, consistent with the current view [22,54–63].

We tentatively attribute the 40% lower yield of Q_A^- formation following 704 nm excitation of the D1:1 variant to a shift of the CT transition to significantly shorter wavelengths, compared to the D1:3 variant. We note that the CT absorption present in the 700–730 nm region in PSII core preparations is absent in isolated D1/D2/Cytb_{559} reaction center preparations prepared from higher plants [42]. An analysis of spectra from D1/D2/Cytb_{559} samples, including Stark data, assigns (Fig. 6 of Novoderhezkin et al. [23]) a CT band peaking near 682 nm having a dipole strength corresponding to ~0.3 Chl *a*. This would indicate that the CT band in D1/D2/Cytb_{559} has moved to significantly higher energy compared to its position in PSII core complexes, presumably due the different effective dielectric and/or charge environment of the P_{D1}/P_{D2} pigments in these preparations. Evidence for a modification of the primary donor between core complex and D1/D2/Cytb_{559} preparations also come from FTIR studies [64,65] used to determine the extent of P^+ delocalization between P_{D1} and P_{D2} (discussed further below).

As discussed in Hughes et al. [19] the low energy CT absorption in PSII core complexes may be composed of more than one CT band. This possibility was introduced to account for the observation that excitation of higher-plant PSII at progressively longer wavelengths leads to a notable drop in the quantum efficiency of Q_A^- formation. It is possible that the different yields and efficiencies of Q_A^- formation following 704 nm excitation of the D1-variants reflect the direct excitation of different CT band components.

The fluorescence yield and thermoluminescence results of Kós et al. [12] were interpreted to indicate that the free energy gap between the $P^+Pheo^-_{D1}$ and P* states, relevant in the kinetic scheme for $S_2Q_A^-$ and $S_2Q_B^-$ recombination, is increased in the D1:3 variant. If the P* energy is considered invariant in the two D1 isoforms [12], then the $P^+Pheo^-_{D1}$ energy has been lowered in D1:3. The long-lived P^+ state is considered to be P^+_{D1} (discussed in more detail below). The interpretation of our data (above) suggests that a P_{D1}–P_{D2} optical CT state is also at lower energy in the D1:3 variant.

4.2. Site-specific effects of D1 variants on $Pheo_{D1}$ and the primary donor

There are 21 amino acid differences in the primary sequence of the D1 polypeptide between the D1:1 and D1:3 variants. These have been recently modeled [13] based on the published 3.0 Å structural data [51]. There are two differences between D1:1 and D1:3 that seem clearly relevant to the present work: (i) the change near the $Pheo_{D1}$ at position 130 from glutamine to glutamate, and (ii) the amino acid changes in the hydrophobic binding pocket of P_{D1}.

The absence of the hydrogen bond to $Pheo_{D1}$ in the D1:1 variant is expected to result in a less stable $Pheo^-_{D1}$ and a higher energy of the $Chl^+_{D1}Pheo^-_{D1}$ radical pair state (compared to that in D1:3). However, the presence or absence of the hydrogen bond to the $Pheo_{D1}$ may have less effect on the energy of the special pair P_{D1}–P_{D2} charge-separated states of the reaction center that give rise to the optical CT transition(s).

The hydrophobic binding pocket of P_{D1} exhibits four amino acid changes between the D1:1 and D1:3 variants at positions 123, 153, 184 and 283. In particular, the hydrophilic Serine at position D1–153 in the D1:1 is replaced by a hydrophobic Alanine in D1:3. It has been suggested [13] that due to the close proximity of residue D1–153 to the carbonyl groups of P_{D1}, Ser153 may provide a preference over Ala153 for the coordination of a water molecule. This change might modify the hydrogen-bonding network near the P_{D1} carbonyl functions, potentially altering the energetics of P_{D1}/P_{D2} charge-separated states. This provides a rationale for the putative blue shift of the CT band in the D1:1 variant. We also note that the other three residues near the P_{D1} binding pocket at positions 123, 184, and 283 could also provide an effect. We suggest that these amino acid variations near the P_{D1} pigment could be a dominant factor determining the energetics of the optical CT transition(s) in PSII. Site-directed mutagenesis experiments may directly target these single residues in both D1:1 and D1:3 variants.

4.3. Efficiency of side-path oxidation

We found a lower efficiency of the terminal side-path oxidation in the D1:1 variant. There also appeared to be some variation in the distribution of terminal side-path donors between D1:1 and D1:3 variants, where the largest effect was for 704 nm excitation of the D1:1 variant. We briefly discuss how the location of the long-lived P^+ state may contribute to these phenomena.

In plant PSII, FTIR [64,65] and ENDOR [66] as well as FTIR on *T. elongatus* [64] and optical difference spectroscopy on D1-His198/D2-His197 mutants of *Synechocystis* PCC6803 (core complexes) [59] have been interpreted to indicate some differential localization of the long-lived P^+ cation between P_{D1} and P_{D2} (see also the review by Rappaport and Diner [55]). The results were used to suggest a ~70–80% localization on one Chl in PSII core complexes, but the FTIR and ENDOR could not determine on which pigment the charge localization was preferred. Furthermore, the FTIR [64,65] was interpreted to suggest that the charge was shared approximately evenly between P_{D1} and P_{D2} in D1/D2/Cytb_{559} preparations, and taken as an indication that the structure of P680 was modified in these samples.

A different location of the P^+ cation would result in a different electron transfer distance from the Car_{D2} branch point of the side-pathway. From the structural model of Loll et al. [51], the increased edge-to-edge distance for localization of the cation on P_{D2} compared to P_{D1} is 24.1 *vs* 21.0 Å, while the distances from P_{D2} and P_{D1} to Q_A are 22.1 *vs* 21.3 Å, respectively. Using the empirical formula of Dutton et al. [67] for long-range electron transfer in proteins, this translates to maximal electron transfer rates for Car_{D2} oxidation by $P680^+$ of 140 and 2 ms, and the $P^+Q_A^-$ direct recombination reaction of 9 and 3 ms, for either P_{D2} or P_{D1}, respectively. Thus, based on distance alone, a decrease in the efficiency of stable Q_A^- formation and side-path oxidation of up to an order of magnitude is reasonable. We note also that at room temperature at pH 9.3 in Mn-depleted PSII, a faster reduction of P^+ in D1:3 compared to D1:1 has been reported [33].

It was recently concluded from mutagenesis studies of the D1:3 variant that the nature of the ligand to P_{D1} is not a critical determinant of the spectroscopic and redox properties of P in *T. elongatus* [33]. It will be relevant to our results on the side-pathway to determine if the same result holds for the D1:1 variant, and also for mutations at position D1–153 that may alter the hydrogen-bonding pattern to the P_{D1} carbonyl functions. Such an investigation will also be relevant in light of the observations here that regard the dominant effect on the optical CT states as being due to amino acids near P_{D1}.

5. Conclusion

Our investigation indicates that the properties of the primary donor in *T. elongatus* may be correlated with differential expression of the D1 protein. We have interpreted our results to suggest a tuning of the transition energy of an optically accessible CT absorption of the

primary donor to higher energy in the low-light D1:1 variant, compared to the high-light D1:3 variant. The relationship of the excitonic and CT excitations is a crucial factor in determining the effectiveness of different charge separation pathways and stabilization events in PSII, as identified in the recent model presented by Novoderezhkin et al. [23]. In light of this, more detailed investigation of the optically accessible charge transfer transition(s) and charge separation dynamics in the D1 variants, particularly following direct excitation of the CT transitions, could be an insightful avenue for future research.

The quantum efficiency distribution for photo-induced side-path oxidation at 8 K exhibits a lower fraction of the higher efficiency component in the D1:1 variant compared to the D1:3 variant. This result suggests a direction for further investigation of possible differentiation in the photoprotective roles of the side-pathway associated with light-dependent differential *psbA* expression.

Acknowledgements

This work was supported by a joint French-Australian Science and Technology (FAST) Programme (Australian DEST grant number FR07001) to AWR and JLH and the European Union Seventh Framework Programme SOLAR-H2 project number 212508. JLH was supported in part by a Human Frontiers Science Program Organization Long-Term Fellowship, LT00710/2008. JLH and AWR acknowledge support from the Research School of Chemistry, Australian National University for Visiting Fellowships. MS and AB were supported in part by the JSPS and CNRS under the Japan-France Research Cooperative Program for funding (MS, AB) and a grant from Nissan Science Foundation (MS).

References

[1] T.J. Wydrzynski, K. Satoh, in: Govindjee (Ed.), Advances in Photosynthesis and Respiration, 22, Springer, Dordrecht, The Netherlands, 2005, p. 786.
[2] Y. Nakamura, T. Kaneko, S. Sato, M. Ikeuchi, H. Katoh, S. Sasamoto, A. Watanabe, M. Iriguchi, K. Kawashima, T. Kimura, Y. Kishida, C. Kiyokawa, M. Kohara, M. Matsumoto, A. Matsuno, N. Nakazaki, S. Shimpo, M. Sugimoto, C. Takeuchi, M. Yamada, S. Tabata, Complete genome structure of the thermophilic cyanobacterium *Thermosynechococcus elongatus* BP-1, DNA Res. 9 (2002) 123–130.
[3] S.A. Bustos, M.R. Schaefer, S.S. Golden, Different and rapid responses of four cyanobacterial psba transcripts to changes in light-intensity, J. Bacteriol. 172 (1990) 1998–2004.
[4] D. Campbell, A.K. Clarke, P. Gustafsson, G. Öquist, Oxygen-dependent electron flow influences photosystem II function and psbA gene expression in the cyanobacterium *Synechococcus* sp PCC 7942, Physiol. Plant 105 (1999) 746–755.
[5] D. Campbell, M.J. Eriksson, G. Öquist, P. Gustafsson, A.K. Clarke, The cyanobacterium *Synechococcus* resists UV-B by exchanging photosystem II reaction-center D1 proteins, Proc. Natl. Acad. Sci. U. S. A. 95 (1998) 364–369.
[6] D. Campbell, G.Q. Zhou, P. Gustafsson, G. Öquist, A.K. Clarke, Electron-transport regulates exchange of two forms of photosystem-II D1 protein in the cyanobacterium *Synechococcus*, EMBO J. 14 (1995) 5457–5466.
[7] A.K. Clarke, A. Soitamo, P. Gustafsson, G. Öquist, Rapid interchange between two distinct forms of cyanobacterial photosystem-II reaction-center protein-D1 in response to photoinhibition, Proc. Natl. Acad. Sci. U. S. A. 90 (1993) 9973–9977.
[8] K. Sippola, E. Kanervo, N. Murata, E.M. Aro, A genetically engineered increase in fatty acid unsaturation in *Synechococcus* sp. PCC 7942 allows exchange of D1 protein forms and sustenance of photosystem II activity at low temperature, Eur. J. Biochem. 251 (1998) 641–648.
[9] N.F. Tsinoremas, M.R. Schaefer, S.S. Golden, Blue and red-light reversibly control psbA expression in the cyanobacterium *Synechococcus* sp strain Pcc-7942, J. Biol. Chem. 269 (1994) 16143–16147.
[10] J. Sander, M. Nowaczyk, M. Kopczak, M. Rögner, in: J.F. Allen, E. Gantt, J.H. Golbeck, B. Osmond (Eds.), Photosynthesis. Energy from the Sun, Springer, Netherlands, 2008, pp. 745–748.
[11] P.B. Kós, Z. Deák, I. Vass, 12th International Symposium on Phototrophic Prokaryotes, Palais Beaumont-Pau-France, 2006, p. 202.
[12] P.B. Kós, Z. Deák, O. Cheregi, I. Vass, Differential regulation of psbA and psbD gene expression, and the role of the different D1 protein copies in the cyanobacterium *Thermosynechococcus elongatus* BP-1, Biochim. Biophys. Acta 1777 (2008) 74–83.
[13] B. Loll, M. Broser, P.B. Kos, J. Kern, J. Biesiadka, I. Vass, W. Saenger, A. Zouni, Modeling of variant copies of subunit D1 in the structure of photosystem II from *Thermosynechococcus elongatus*, Biol. Chem. 389 (2008) 609–617.
[14] C.I. Sicora, C.M. Brown, O. Cheregi, I. Vass, D.A. Campbell, The psbA gene family responds differentially to light and UVB stress in Gloeobacter violaceus PCC 7421, a deeply divergent cyanobacterium, Biochim. Biophys. Acta 1777 (2008) 130–139.
[15] G. Öquist, D. Campbell, A.K. Clarke, P. Gustafsson, The cyanobacterium *Synechococcus* modulates photosystem II function in response to excitation stress through D1 exchange, Photosynth. Res. 46 (1995) 151–158.
[16] C.I. Sicora, S.E. Appleton, C.M. Brown, J. Chung, J. Chandler, A.M. Cockshutt, I. Vass, D.A. Campbell, Cyanobacterial psbA families in *Anabaena* and *Synechocystis* encode trace, constitutive and UVB-induced D1 isoforms, Biochim. Biophys. Acta 1757 (2006) 47–56.
[17] K. Cser, I. Vass, Radiative and non-radiative charge recombination pathways in photosystem II studied by thermoluminescence and chlorophyll fluorescence in the cyanobacterium *Synechocystis* 6803, Biochim. Biophys. Acta 1767 (2007) 233–243.
[18] S.A.P. Merry, P.J. Nixon, L.M.C. Barter, M. Schilstra, G. Porter, J. Barber, J.R. Durrant, D.R. Klug, Modulation of quantum yield of primary radical pair formation in photosystem II by site-directed mutagenesis affecting radical cations and anions, Biochemistry 37 (1998) 17439–17447.
[19] J.L. Hughes, P. Smith, R. Pace, E. Krausz, Charge separation in photosystem II core complexes induced by 690–730 nm excitation at 1.7 K, Biochim. Biophys. Acta 1757 (2006) 841–851.
[20] M. Szczepaniak, J. Sander, M. Nowaczyk, M.G. Müller, M. Rögner, A.R. Holzwarth, Charge separation, stabilization, and protein relaxation in photosystem II core particles with closed reaction center, Biophys. J. 96 (2009) 621–631.
[21] G. Raszewski, T. Renger, Light harvesting in photosystem II core complexes is limited by the transfer to the trap: can the core complex turn into a photoprotective mode? J. Am. Chem. Soc. 130 (2008) 4431–4446.
[22] A.R. Holzwarth, M.G. Müller, M. Reus, M. Nowaczyk, J. Sander, M. Rögner, Kinetics and mechanism of electron transfer in intact photosystem II and in the isolated reaction center: pheophytin is the primary electron acceptor, Proc. Natl. Acad. Sci. U. S. A. 103 (2006) 6895–6900.
[23] V.I. Novoderezhkin, J.P. Dekker, R. van Grondelle, Mixing of exciton and charge-transfer states in photosystem II reaction centers: modeling of stark spectra with modified redfield theory, Biophys. J. 93 (2007) 1293–1311.
[24] V.L. Novoderezhkin, E.G. Andrizhiyevskaya, J.P. Dekker, R. van Grondelle, Pathways and timescales of primary charge separation in the photosystem II reaction center as resolved by a simultaneous fit of time-resolved fluorescence and transient absorption, Biophys. J. 89 (2005) 1464–1481.
[25] S. Vassiliev, C.-I. Lee, G.W. Brudvig, D. Bruce, Structure-based kinetic modeling of excited-state transfer and trapping in histidine-tagged photosystem II core complexes from *Synechocystis*, Biochemistry 41 (2002) 12236–12243.
[26] L. Konermann, G. Gatzen, A.R. Holzwarth, Primary processes and structure of the photosystem II reaction center. 5. Modeling of the fluorescence kinetics of the D_1–D_2–cyt-b_{559} complex at 77 K, J. Phys. Chem. B 101 (1997) 2933–2944.
[27] S. Styring, A.W. Rutherford, Deactivation kinetics and temperature dependence of the S-state transitions in the oxygen-evolving system of photosystem II measured by EPR spectroscopy, Biochim. Biophys. Acta 933 (1988) 378–387.
[28] D.H. Stewart, G.W. Brudvig, Cytochrome b_{559} of photosystem II, Biochim. Biophys. Acta 1367 (1998) 63–87.
[29] P. Faller, C. Fufezan, A.W. Rutherford, in: T.J. Wydrzynski, K. Satoh (Eds.), Photosystem II — The Light-Driven Water:Plastoquinone Oxidoreductase, Springer, Dordrecht, The Netherlands, 2005, pp. 347–365.
[30] J. Hanley, Y. Deligiannakis, A. Pascal, P. Faller, A.W. Rutherford, Carotenoid oxidation in photosystem II, Biochemistry 38 (1999) 8189–8195.
[31] J.L. Hughes, A.W. Rutherford, M. Sugiura, E. Krausz, Quantum efficiency distributions of photo-induced side-pathway donor oxidation at cryogenic temperature in photosystem II, Photosynth. Res. 98 (2008) 199–206.
[32] M. Sugiura, Y. Inoue, Highly purified thermo-stable oxygen-evolving photosystem II core complex from the thermophilic cyanobacterium *Synechococcus elongatus* having His-tagged CP43, Plant Cell Physiol. 40 (1999) 1219–1231.
[33] M. Sugiura, A. Boussac, T. Noguchi, F. Rappaport, Influence of Histidine-198 of the D1 subunit on the properties of the primary electron donor, P-680, of photosystem II in *Thermosynechococcus elongatus*, Biochim. Biophys. Acta 1777 (2008) 331–342.
[34] J.L. Hughes, E. Krausz, in: R.A. Scott, C.M. Lukehart (Eds.), Applications of Physical Methods to Inorganic and Bioinorganic Chemistry, John Wiley & Sons, Ltd., New York, 2007, pp. 79–98.
[35] R. Stranger, L. Dubicki, E. Krausz, Magneto-optical investigation of the exchange-coupled dimer $Cs_3Mo_2Br_9$, Inorg. Chem. 35 (1996) 4218–4226.
[36] R. Steffen, K. Jackman, E.R. Krausz, Design and application of a high-precision, broad spectral range CCD-based absorption spectrometer with millisecond time resolution, Meas. Sci. Technol. 19 (2008) 075601.
[37] E.J. Bylina, C. Kirmaier, L. McDowell, D. Holten, D.C. Youvan, Influence of an amino-acid residue on the optical properties and electron transfer dynamics of a photosynthetic reaction center complex, Nature 336 (1988) 182–184.
[38] D.H. Stewart, P.J. Nixon, B.A. Diner, G.W. Brudvig, Assignment of the Q_y absorbance bands of photosystem II chromophores by low-temperature optical spectroscopy of wild-type and mutant reaction centres, Biochemistry 39 (2000) 14583–14594.
[39] L.B. Giorgi, P.J. Nixon, S.A.P. Merry, D.M. Joseph, J.R. Durrant, J.D. Rivas, J. Barber, G. Porter, D.R. Klug, Comparison of primary charge separation in the photosystem II reaction center complex isolated from wild-type and D1–130 mutants of the cyanobacterium *Synechocystis* PCC 6803, J. Biol. Chem. 271 (1996) 2093–2101.
[40] W.L. Butler, Primary photochemistry of photosystem II of photosynthesis, Acc. Chem. Res. 6 (1973) 177–184.
[41] N. Cox, J.L. Hughes, R. Steffen, P.J. Smith, A.W. Rutherford, R.J. Pace and E. Krausz, Identification of the Qy excitation of the primary electron acceptor of photosystem II: CD determination of its coupling environment, J. Phys. Chem. B (2009), doi:10.1021/jp808796x.

[42] E. Krausz, N. Cox, S. Peterson Årsköld, Spectral characteristics of PS II reaction centres: as isolated preparations and when integral to PS II core complexes, Photosynth. Res. 98 (2008) 207–217.
[43] J.L. Hughes, B. Conlan, T. Wydrzynski and E. Krausz, Physics Procedia (submitted for publication).
[44] S.G. Boxer, Stark realities, J. Phys. Chem. B 113 (2009) 2972–2983.
[45] J.L. Hughes, P.J. Smith, R.J. Pace, E. Krausz, Spectral hole-burning at the low-energy absorption edge of photosystem II core complexes, J. Lumin. 119–120 (2006) 298–303.
[46] E. Krausz, J.L. Hughes, P. Smith, R. Pace, S. Peterson Årsköld, Oxygen-evolving photosystem II core complexes: a new paradigm based on the spectral identification of the charge-separating state, the primary acceptor and assignment of low-temperature fluorescence, Photochem. Photobiol. Sci. 4 (2005) 744–753.
[47] J.L. Hughes, B.J. Prince, E. Krausz, P.J. Smith, R.J. Pace, H. Riesen, Highly efficient spectral hole-burning in oxygen-evolving photosystem II preparations, J. Phys. Chem. B 108 (2004) 10428–10439.
[48] J.L. Hughes, P.J. Smith, R.J. Pace, E. Krausz, Low energy absorption and luminescence of higher plant photosystem II core samples, J. Lumin. 122–123 (2007) 284–287.
[49] J.L. Hughes, E. Krausz, Novel characteristics of persistent spectral hole-burning and hole-filling in photosystem II core complexes, J. Lumin. 127 (2007) 239–244.
[50] J.L. Hughes, E. Krausz, P.J. Smith, R.J. Pace, H. Riesen, Probing the lowest energy chlorophyll *a* states of photosystem II via selective spectroscopy: new insights on P680, Photosynth. Res. 84 (2005) 93–98.
[51] B. Loll, J. Kern, W. Saenger, A. Zouni, J. Biesiadka, Towards complete cofactor arrangement in the 3.0 Å resolution crystal structure of photosystem II, Nature 438 (2005) 1040–1044.
[52] K.N. Ferreira, T.M. Iverson, K. Maghlaoui, J. Barber, S. Iwata, Architecture of the photosynthetic oxygen-evolving center, Science 303 (2004) 1831–1838.
[53] W.W. Parson, A. Warshel, Spectroscopic properties of photosynthetic reaction centres. 2. Application of the theory to *Rhodopseudomonas viridis*, J. Am. Chem. Soc. 109 (1987) 6152–6163.
[54] G. Raszewski, B.A. Diner, E. Schlodder, T. Renger, Spectroscopic properties of reaction center pigments in photosystem II core complexes: revision of the multimer model, Biophys. J. 95 (2008) 105–119.
[55] F. Rappaport, B.A. Diner, Primary photochemistry and energetics leading to the oxidation of the (Mn)4Ca cluster and to the evolution of molecular oxygen in photosystem II, Coord. Chem. Rev. 252 (2008) 259–272.
[56] M.L. Groot, N.P. Pawlowicz, L.J.G.W. van Wilderen, J. Breton, I.H.M. van Stokkum, R. van Grondelle, Initial electron donor and acceptor in isolated photosystem II reaction centers identified with femtosecond mid-IR spectroscopy, Proc. Natl. Acad. Sci. U. S. A. 102 (2005) 13087–13092.
[57] G. Raszewski, W. Saenger, T. Renger, Theory of optical spectra of photosystem II reaction centers: location of the triplet state and the identity of the primary electron donor, Biophys. J. 88 (2005) 986–998.
[58] B.A. Diner, F. Rappaport, Structure, dynamics, and energetics of the primary photochemistry of photosystem II of oxygenic photosynthesis, Annu. Rev. Plant Biol. 53 (2002) 551–580.
[59] B.A. Diner, E. Schlodder, P.J. Nixon, W.J. Coleman, F. Rappaport, J. Lavergne, W.F.J. Vermaas, D.A. Chisholm, Site-directed mutations at D1-His198 and D2-His197 of photosystem II in *Synechocystis* PCC 6803: sites of primary charge separation and cation and triplet stabilization, Biochemistry 40 (2001) 9265–9281.
[60] V.I. Prokhorenko, A.R. Holzwarth, Primary processes and structure of the photosystem II reaction center: a photon echo study, J. Phys. Chem. B 104 (2000) 11563–11578.
[61] J.P. Dekker, R. van Grondelle, Primary charge separation in photosystem II, Photosynth. Res. 63 (2000) 195–208.
[62] A.W. Rutherford, in: S.E. Stevens, D.A. Bryant (Eds.), Light Energy Transduction in Photosynthesis: Higher Plant and Bacterial Models, The American Society of Plant Physiologists, Rockville, 1988, pp. 163–177.
[63] F.J.E. van Mieghem, K. Satoh, A.W. Rutherford, A chlorophyll tilted 30-degrees relative to the membrane in the photosystem-II reaction center, Biochim. Biophys. Acta 1058 (1991) 379–385.
[64] T. Okubo, T. Tomo, M. Sugiura, T. Noguchi, Perturbation of the structure of P680 and the charge distribution on its radical cation in isolated reaction center complexes of photosystem II as revealed by Fourier transform infrared spectroscopy, Biochemistry 46 (2007) 4390–4397.
[65] T. Noguchi, T. Tomo, Y. Inoue, Fourier transform infrared study of the cation radical of P680 in the photosystem II reaction center: evidence for charge delocalization on the chlorophyll dimer, Biochemistry 37 (1998) 13614–13625.
[66] S.E.J. Rigby, J.H.A. Nugent, P.J. O'Malley, ENDOR and special triple resonance studies of chlorophyll cation radicals in photosystem 2, Biochemistry 33 (1994) 10043–10050.
[67] C.C. Page, C.C. Moser, X. Chen, P.L. Dutton, Natural engineering principles of electron tunnelling in biological oxidation–reduction, Nature 402 (1999) 47–52.